applied sciences

MDPI

Article

Analysis of a Nature-Inspired Shape for a Vertical Axis Wind Turbine

Javier Blanco Damota [1], Juan de Dios Rodríguez García [1], Antonio Couce Casanova [1], Javier Telmo Miranda [2], Claudio Giovanni Caccia [3] and María Isabel Lamas Galdo [1,*]

[1] Escuela Politécnica de Ingeniería de Ferrol, Universidade da Coruña, 15403 Ferrol, Spain; javier.blanco.damota@udc.es (J.B.D.); de.dios.rodriguez@udc.es (J.d.D.R.G.); antonio.coucec@udc.es (A.C.C.)
[2] Escuela Técnica Superior de Ingenieros Industriales, UNED, 28040 Madrid, Spain; jtelmo@ieec.uned.es
[3] Department of Aerospace Engineering, Politecnico di Milano, 20156 Milan, Italy; claudiogiovanni.caccia@polimi.it
* Correspondence: isabel.lamas.galdo@udc.es; Tel.: +34-881013896

Abstract: Wind energy is gaining special interest worldwide due to the necessity of reducing pollutant emissions and employ renewable resources. Traditionally, horizontal axis wind turbines have been employed but certain situations require vertical axis wind turbines. With a view to improve the efficiency of a vertical axis wind turbine Savonius type, the present work proposes a bioinspired design blade profile relying on the Fibonacci spiral. This shape is repeatedly presented in nature and thus it leads to a bio-inspired blade profile. A numerical model was carried out and it was found that the Fibonacci shape improves the performance of the original Savonius shape, based on semicircular blade profiles. Particularly, the Fibonacci blade profile increases around 14% the power in comparison with the Savonius blade profile. Besides this comparison between Savonius and Fibonacci, a research study was carried out to improve the efficiency of the Fibonacci turbine. To this end, the effect of several parameters was analyzed: number of blades, aspect ratio, overlap, separation gap, and twist angle. Improvements on the average power greater than 30% were obtained.

Keywords: wind turbine; VAWT; CFD; Savonius; Fibonacci

Citation: Damota, J.B.; García, J.d.D.R.; Casanova, A.C.; Miranda, J.T.; Caccia, C.G.; Galdo, M.I.L. Analysis of a Nature-Inspired Shape for a Vertical Axis Wind Turbine. *Appl. Sci.* **2022**, *12*, 7018. https://doi.org/10.3390/app12147018

Academic Editor: Michal Puškár

Received: 20 June 2022
Accepted: 10 July 2022
Published: 12 July 2022

1. Introduction

The continuously growing energy demand constitutes an important issue for society. The main fossil resources currently employed for power generation, such as natural gas, coal, oil, etc., generate a significant level of pollutants; moreover, these fuels are non-renewable resources. These facts have incremented the interest in renewable energies. Among all types of renewable energies, wind energy has experienced a rapid growth over the last years. It is expected that wind energy will account more than 40% of all renewable energy by 2030 [1] and 20% of the worldwide energy demand [2].

According to the orientation of the rotating axis, two types of wind turbines can be distinguished: Horizontal Axis Wind Turbines (HAWT) and Vertical Axis Wind Turbines (VAWT). HAWTs have a rotating axis parallel to the wind direction. These are the most common wind turbines, employed in high power farms, although can also be found in small sizes for mini wind power applications. On the other hand, VAWT have a rotating axis perpendicular to the wind direction. These wind turbines are less common but nowadays are the focus of much research due to their low power applications. The growing worldwide demand for wind energy leads to the necessity of obtaining a more efficient use of wind that cannot be employed by large HAWTs. To this end, VAWTs are aimed at low scale applications, especially urban environments with poor wind conditions [3–6]. The exploitation of these winds together with the winds exploited by large wind turbines may considerably increase the global wind energy production.

Regarding VAWTs, two types can be found in the literature. The Darrieus turbine, mainly based on lift, and the Savonius turbine, mainly based on drag. The main propulsor effect in the Savonius turbines is the drag force acting on them, while the Darrieus rotating principle is mainly based on the lift force actuating on the blades. The Savonius wind turbine was initially proposed by Sigur Savonius [7] in the 1930s. This turbine is integrated by two semi-circular sections vertically positioned along the rotation axis. The main advantages are its simplicity, high start-up, low noise, and independence of the wind direction [8]. In comparison with a Darrieus turbine, the Savonius is more recommended for urban environments due to its lower starting torque, i.e., it needs lower wind velocities for starting. In offshore applications, the Savonius turbine is appropriated as a hydrokinetic turbine to generate energy from tidal currents [9–12]. Despite these advantages, the main disadvantage of the Savonius turbine is its low efficiency [13,14]. For this reason, these types of turbines have been scarcely employed until recent decades. Many modifications have been proposed along the years in order to increment the efficiency of the Savonius turbine. The most significant parameters analyzed in the scientific literature (number of blades, aspect ratio, overlap, separation gap, and twist angle) are analyzed below, and a schematic representation of them is shown in Figure 1.

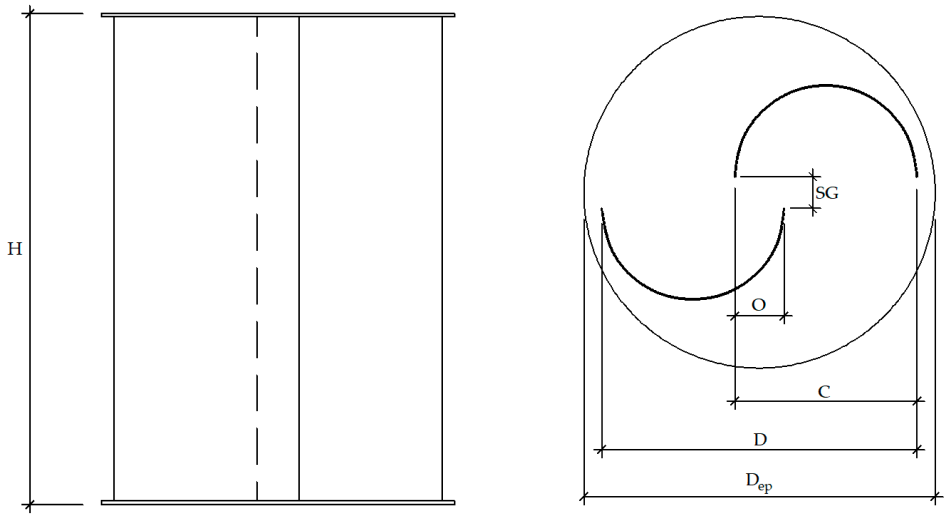

Figure 1. Savonius turbine; (**a**) 3D view; (**b**) lateral section. H: height, C: chord length, O: overlap, SG: separation gap, D: rotor diameter, D_{ep}: end plate diameter.

1.1. Aspect Ratio

The aspect ratio is the relation between the height and the rotor diameter, i.e., AR = H/D. Important discrepancies can be found in the literature regarding the optimum value of this parameter. While some researchers propose 2 as the optimum aspect ratio [12], other researches established the optimum AR around 4 [15–17], and even higher values such as 6 [18].

1.2. Overlap

The overlap is the distance that an inside edge penetrates into another. This parameter has been extensively studied due to its importance on power generation. As in the previous case regarding the aspect ratio, different values were proposed as optimum and important discrepancies can be found in the literature. One can refer to Sheldahl et al. [19], who proposed 10–15% of the chord length as optimum overlap value; Fujisawa [20], who proposed 15% of the chord length; Mojola [21] and Alexander and Holownia [13], who proposed 20–30% of the chord length; and Menet and Bourabaa [22], who analyzed both the aspect ratio and overlap and established an optimum overlap as 24.2% when AR = 2.

1.3. Separation Gap

The separation gap is the width separating the inside edges of the blades. Several studies analyzed the effect of the separation gap and most of them concluded that the optimum value is zero [12] since increments in the separation gap reduce the power of the wind turbine due to reductions in the quantity of air in the blade opposed to the movement.

1.4. Number of Blades

Many researchers concluded that the optimum number of blades is two [16,18] since the power is reduced when the number of blades increases. Nevertheless, an advantage of turbines with more than two blades is that the starting torque is lower [19]. This is especially important under low velocity wind conditions, where turbines with more than two blades are appropriate although they provide less efficiency.

1.5. Twist Angle

The twist angle is the angle between the upper and lower sections of the blades, Figure 2. Lee et al. [23] analyzed 0°, 45°, 90°, and 135° twist angles and found that the optimum value is 45°. Zhao et al. [18] analyzed 90°, 180°, 270°, and 360° and found that the optimum value is 180°. Damak et al. [24,25] compared two Savonius turbines with 0° and 180° twist angles and found that the latter provided higher power coefficients.

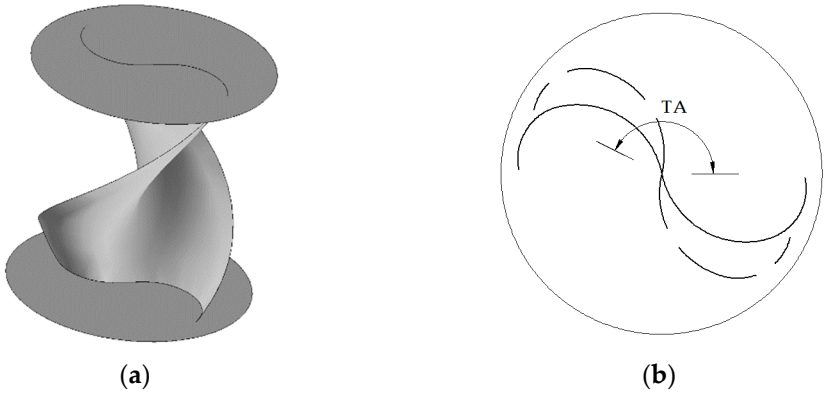

Figure 2. Twist angle; (**a**) 3D view; (**b**) upper view.

1.6. Blade Profile

One of the most significant improvements proposed in the literature consists of employing blade profiles different from the semicircular profile initially proposed by Sigur Savonius [7]. Some examples are the models of Kumar et al. [26], Alom and Saha [27], Kacprzak et al. [28], Benesh [29], Mohamed et al. [30], and Chan et al. [31], as illustrated in Figure 3a,f, respectively.

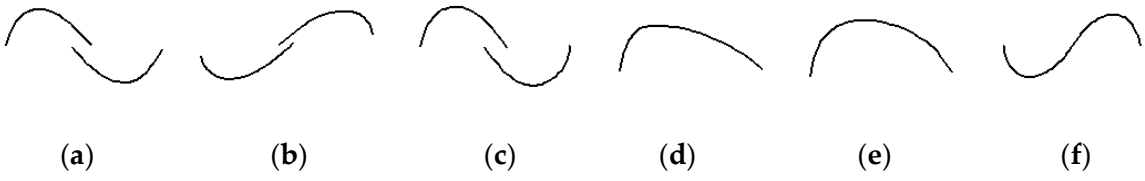

Figure 3. Some modified profiles proposed in the literature; (**a**) Kumar et al. [26]; (**b**) Alom and Saha [27]; (**c**) Kacprzak et al. [28]; (**d**) Benesh [29]; (**e**) Mohamed et al. [30]; (**f**) Chan et al. [31].

The present work proposes an innovative nature-inspired blade profile based on the Fibonacci sequence. Geometrically, this sequence constitutes a spiral that is presented in many natural contexts such as vegetables, animals, and nature phenomena in general, as shown in Figure 4. Since the Fibonacci spiral is highly presented in nature, and thus is consequence of millions of years of evolution, it is appropriate to propose this geometry

for VAWT wind turbines, obtaining a bio-inspired blade profile. In relation to this, some authors of the present work have proposed a bio-inspired shape for a marine propulsor elsewhere [32–35], improving the performance of the traditional propellers for certain applications. These works demonstrate that sometimes nature can appropriately inspire mechanical devices with surprising results.

(**a**) (**b**) (**c**)

Figure 4. Examples of the Fibonacci spiral in nature. (**a**) Snail shell; (**b**) Fran hurricane, September 1996 [36]; (**c**) Whirlpool Galaxy [37].

The Fibonacci blade profile proposed in the present work and its modifications to improve the performance were analyzed numerically. In a previous work [38], the Fibonacci shape was proposed to investigate the effect of number of blades, aspect ratio, overlap, separation gap, and twist angle. The present work aims to analyze the effect of these parameters. To this end, a numerical model was carried out based on CFD (Computational Fluid Dynamics). This model was validated with experimental measurements obtained elsewhere [20].

2. Materials and Methods

2.1. Numerical Model

As mentioned previously, a numerical model was developed to analyze several modifications of a VAWT Savonius type. Numerical models present important advantages over experimental setups. Contrary to the high cost and time necessaries to carry out experimental measurements of different configurations, the CFD model developed constituted a tool to fast and cheaply analyze different geometries performance parameters. Moreover, numerical models provide interesting information regarding the velocity and pressure field that are too complicated to measure experimentally.

The software OpenFOAM was employed. The main reason is that this is an open source and thus it allows a total access to the code to understand and manipulate it. The governing equations are the RANS (Reynolds-averaged Navier–Stokes). In particular, the conservation of mass and momentum were implemented. As a turbulence model, the SST k-ω was employed since several studies revealed its estimation capabilities in VAWTs [39–43]. In a previous work [44], several turbulence models were compared, and it was concluded that the SST k-ω is the most appropriate for these simulations although the computational cost was higher than other turbulence models, such as the commonly employed k-ε. The PIMPLE algorithm was employed for the pressure–velocity coupling. The temporal treatment was realized through an implicit method, with a constant time step corresponding to 1° of rotation. In order to reach a quasi-state state, several revolutions must be analyzed. Particularly, the results shown in the present work refer to the 6th rotation.

When modeling wind turbines, it is common to employ the non-dimensional parameters shown in Equations (1)–(3).

$$\mathrm{TSR} = \frac{\text{blade tip tangential velocity}}{\text{wind speed}} = \frac{\omega R}{V} \tag{1}$$

$$C_p = \frac{P}{P_{available}} = \frac{P}{0.5\,\rho S V^3} \tag{2}$$

$$C_T = \frac{T}{T_{available}} = \frac{T}{0.25\ \rho S V^2 D} \quad (3)$$

In the equations above, V is the undisturbed wind speed, ω the rotational speed, P the power, ρ the density of air, S the cross section area (S = DH), T the torque, C_T the torque coefficient, and C_P the power coefficient. TSR is the ratio between the blade tip tangential velocity and the wind speed. The power coefficient represents which fraction of the power in the wind is being extracted by the turbine through the projected area of the rotor at the flow direction. The mass flow rate for an air stream flowing through a surface S is ρSV, and therefore the available power comes from its kinetic energy, i.e., $P_{available} = 0.5\ \rho V S V^2 = 0.5\ \rho S V^3$. The power coefficient represents the ratio of the power to the available power. The available torque for an air stream is $T_{available} = P_{available}/\omega$. Taking into account that $V = \omega R$, the latter expression yields that $T_{available} = P_{available}/\omega = 0.5\ \rho S V^3/(V/R) = 0.5\ \rho V S V^2/(2\ V/D) = 0.25\ \rho S V^2 D$. The torque coefficient represents the ratio of the torque to the available torque, as shown in Equation (3). Obviously, since the power is $P = T \cdot \omega$, in non-dimensional form it holds that $C_P = C_T.TSR$, as can be seen in Equation (4).

$$C_p = \frac{P}{P_{available}} = \frac{P}{0.5\ \rho S V^3} = \frac{T\omega}{0.5\ \rho S V^3} = C_T TSR \quad (4)$$

The domain and boundary conditions are shown in Figure 5. The dimensions are 23 × 8 × 8 m. It was verified that these dimensions are large enough to avoid any border effect. This was checked repeating the simulation using domains 10 × 10 × 25 m and 12 × 12 × 30 m and obtaining the same results. The boundary conditions are also shown in this figure. The upstream face was modeled as a velocity inlet, while the downstream face was modeled as an outlet. The exterior faces were modeled as free slip in order to minimize border effects. This boundary condition imposes a zero shear stress, i.e., the tangential velocity derivative normal to the boundary is zero. The turbine blades were treated as no-slip surfaces.

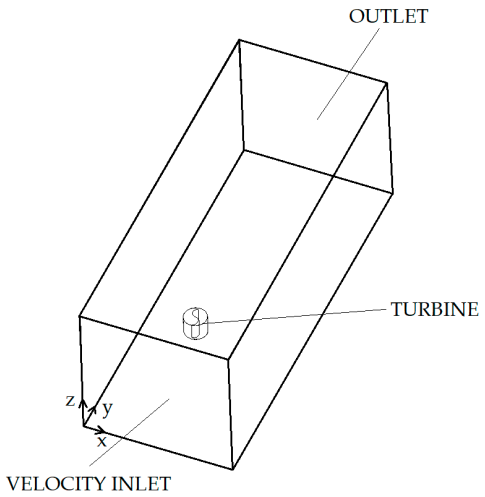

Figure 5. Boundary conditions.

The mesh is shown in Figure 6. This figure shows a tri-dimensional view and a detail of the middle plane. The mesh consists of tetrahedral elements from 0.05 to 0.2 m size. The size is finer around the turbine. Two zones were established: static and rotating. The rotating domain is a cylinder around the turbine which rotates around the turbine axis. The static domain is the remaining region, which remains fixed. A sliding interface connects the static and rotating domains.

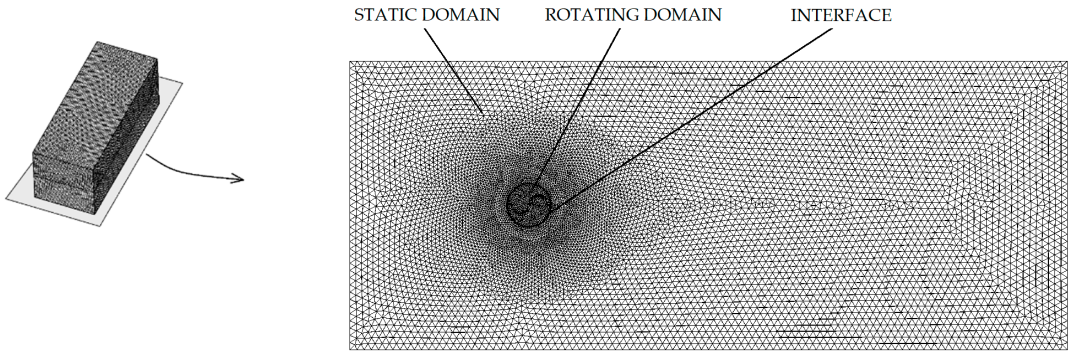

Figure 6. 3D computational mesh and detail of the middle plane.

Several meshes with different elements were tested in order to verify that the results are independent of the mesh size. Table 1 indicates the power coefficient obtained at TSR = 1 using four meshes. It can be seen that meshes 3 and 4 provide the same result. According to this, mesh 3 was selected.

Table 1. Computational meshes checked.

Mesh	Number of Elements	C_P at TSR = 1
Mesh 1	1.5×10^6	0.226
Mesh 2	2.9×10^6	0.212
Mesh 3	3.8×10^6	0.207
Mesh 4	4.5×10^6	0.207

Regarding the near wall cells, a boundary layer with five layers was established, providing a y^+ lower than 1.

2.2. Validation of the Results

In order to validate the model, the numerical results were compared to experimental measurements of Sandia laboratories [20]. To this end, a turbine with the parameters indicated in Figure 7 was analyzed. It can be seen that this turbine is composed of two semi-circular blades and two support endplates. There is a consensus in the literature regarding the optimal size of the endplates, around 1.1 times the rotor diameter. The reason is that very high diameters increase rotor inertia [12].

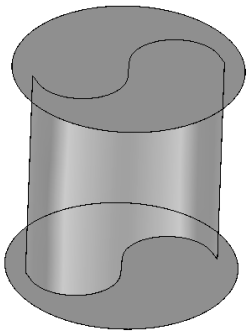

Parameter	Value
Diameter (m)	1
Height (m)	1
Number of blades	2
Overlap (m)	0
Separation gap (m)	0
Twist angle (°)	0

Figure 7. Characteristics of the turbine used for the validation procedure.

The average power coefficient against the tip speed ratio obtained numerically and experimentally are shown in Figure 8. It can be seen that a satisfactory concordance was obtained. It is noteworthy that the average error between numerical and experimental results is 5.8%. Both results show a similar trend, with increments of the average power

coefficients and, after a certain value, decreases with the increase of the tip speed ratio. The reason is that when the tip speed ratio increases, and thus the rotation velocity, the velocity of the blade tips exceeds the air velocity and less power is transferred from the wind to the turbine, reducing the net power. Several reasons may explain the small discrepancies obtained between experimental and numerical results. On the one hand, CFD is not an exact science and discretization is applied to the mesh and governing equations. On the other hand, experimental methods have an inevitable tolerance. Moreover, another important source of error is due to the blockage effect. The blockage effect is caused by employing a wind tunnel with limited dimensions. The flow is restricted around the turbine and cause a local acceleration of the wind velocity in the test section which increments the drag and the measured power coefficient. Blackwell et al. [20] propose a blockage correction factor, also called velocity increment factor, to correct the experimental measurements, but they highlight that the validity of the factor employed is questionable and it is necessary to deeply analyze corrections factors for Savonius turbines. More recently, Ross and Altman [45] compared several blockage corrections for Savonius turbines and concluded that the methodology employed by Blackwell et al. [20] is appropriate.

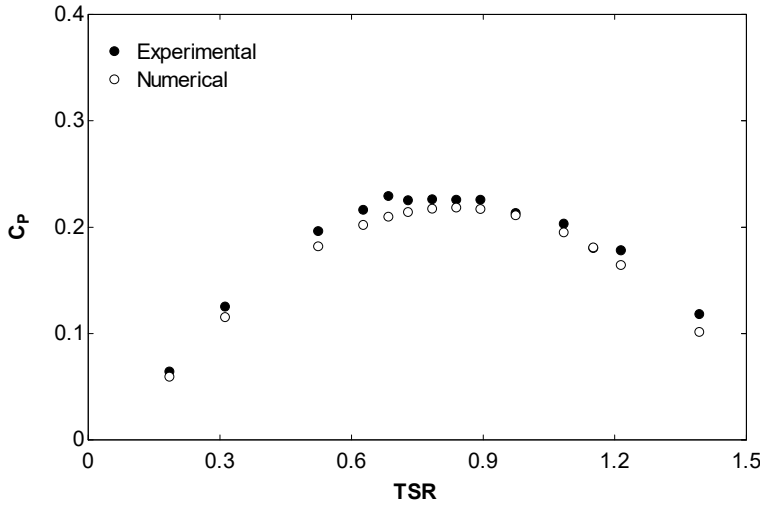

Figure 8. C_P against TSR experimentally and numerically obtained.

3. Results and Discussion

As the numerical model has been validated, a new blade profile based on a naturally-inspired shape, the Fibonacci spiral, is proposed in Section 3.1. Subsequently, the effects of several parameters on the Fibonacci blade profile are analyzed in Section 3.2. The objective of Section 3.2 is to improve the performance of the Fibonacci blade profile.

3.1. Fibonacci Sequence

The Fibonacci numbers were first described in 200 BC by Indian mathematicians [46]. In the Middle Ages, they were analyzed by the Italian mathematician Leonardo of Pisa, who was known as Fibonacci (Fillus Bonacci, i.e., the son of Bonacci). The Fibonacci sequence is a recurrent succession given by Equations (5)–(7), where each term f depends on the two predecessors, $n - 1$ and $n - 2$.

$$f_0 = 0 \tag{5}$$

$$f_1 = 1, \text{ if } n = 1 \tag{6}$$

$$f_n = f_{n-2} + f_{n-1}, \text{ if } n > 1 \tag{7}$$

The Fibonacci spiral is based on the Fibonacci sequence. The graphical representation of the Fibonacci sequence consists of establishing squares with the size of the successive terms, situated as shown in Figure 9. The Fibonacci spiral is also shown in this figure,

which is formed by circumference arcs. Following the Fibonacci sequence, the side sizes of these squares are 0, 1, 1, 2, 3, 5, 8, 13, 21, 34, 55, 89, etc.

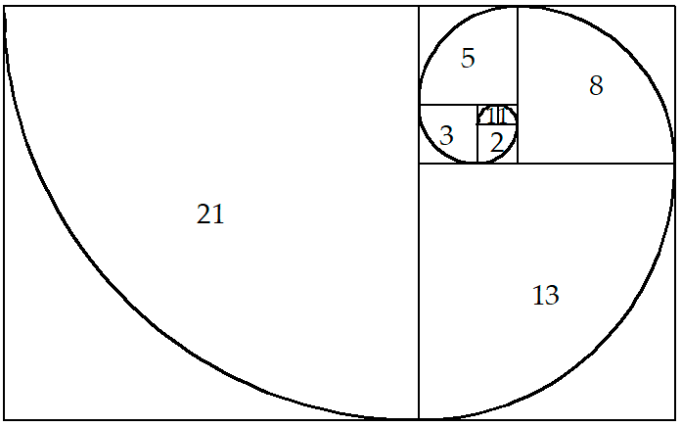

Figure 9. Fibonacci spiral obtained from the Fibonacci sequence.

The blade profile proposed in the present work is composed by two consecutive sections of the Fibonacci spiral. Any consecutive terms high enough lead to the same relation, the so-called golden ratio or divine proportion [47], 1.61803398874986. The higher the consecutive terms, the closer their relationship to the golden ratio, as shown in Equation (8).

$$\frac{f_n}{f_{n-1}} = 1.618033988749864\ldots \text{ if } n \to \infty, \text{ if } n > 1 \quad (8)$$

According to this, each blade is composed by two curves whose ratios are related by the golden ratio. Depending on the orientation, two possibilities can be applied (sequence low-high-high-low or sequence high-low-low-high), shown in Figure 10a,b. For comparison purposes, the semicircular Savonius blade profile is also illustrated in these figures though dotted lines.

(**a**) (**b**)

Figure 10. Blade profiles analyzed; (**a**) Fibonacci I (black color dashed line), sequence low-high-high-low, and comparison with Savonius (grey color dotted line); (**b**) Fibonacci II (black color dashed line), sequence high-low-low-high, and comparison with Savonius (grey color dotted line).

Figure 11a illustrates the average power coefficient and Figure 11b the average thrust coefficient against the tip speed ratio for both Fibonacci blade profiles proposed and the Savonius blade profile. It can be seen that both the power and thrust coefficient increase with the tip speed ratio up to a certain value after which it drops down. Fibonacci I configuration provides a higher power and thrust coefficient than Savonius one. Particularly, a 14.1% improvement on the average power coefficient was obtained and a 13.5% improvement on the average thrust coefficient. Nevertheless, Fibonacci II configuration provides lower power and thrust coefficients. Due to this, the Fibonacci I blade profile will be adopted in the remaining work. The reason of the results obtained in Figure 11 is the principle of operation of a Savonius turbine. The power is mainly produced by drag, and the Fibonacci I configuration increments the drag force of the advancing blade and reduces the drag force of the returning blade, increasing the net driving force.

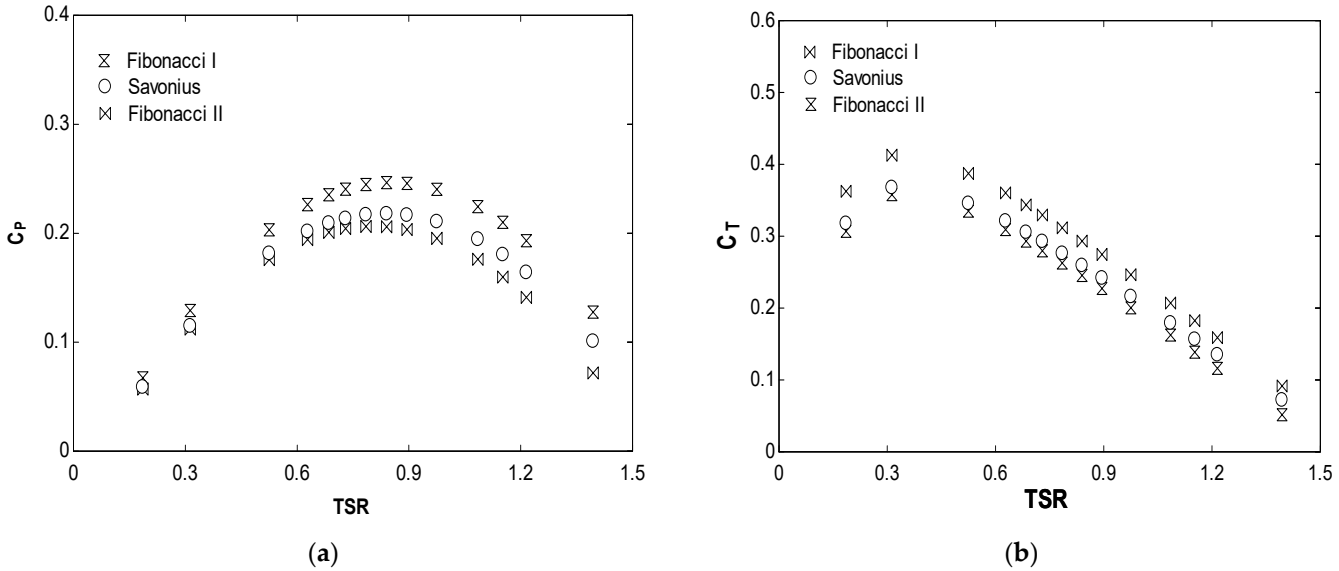

Figure 11. (**a**) C_P against TSR for Savonius, Fibonacci I, and Fibonacci II blade profiles; (**b**) C_T against TSR for Savonius, Fibonacci I, and Fibonacci II blade profiles.

Other improvements obtained by different authors are summarized in Table 2. It is worth mentioning that C_P varies with the Reynolds number. For this reason, it is difficult to compare which shape is the most appropriate using this table since all data should be analyzed under the same Reynolds number.

Table 2. Results of blade shape modification of the Savonius turbine.

Blade Profile	C_P Improvement (%)	Reference
Batch	10.5	[48]
Elliptical	10.3	[28]
Airfoil	10	[49]
Elliptical	17.81	[50]
Elliptical	8.89	[51]
Elliptical	11.34	[52]

Another interest aspect is related to the turbine fatigue hazard. Many VAWTs fail due to blending. The responsible stresses are cyclic and thus promote fatigue, and a dimensional parameter related to the fatigue damage is C_F, Equation (9), where F represents the thrust force. Since the torque is T = F·R, in non-dimensional form it holds that $C_T = C_F$.

$$C_F = \frac{\mathbf{F}}{0.5\ \rho S V^2} \tag{9}$$

According to this, it is important to minimize both thickness and thrust loading. To this end, the parameter SC_{Pmax}, Equation (10) [53], represents the superiority of the maximum C_P.

$$SC_{Pmax} = \frac{C_{Pmax}}{C_F} \times \%t \tag{10}$$

In the equation above, %t represents the thickness of the blade as percentage of the chord length. For instance, using a 5% thickness, the results corresponding to Savonius, Fibonacci I, and Fibonacci II are shown in Table 3. It can be seen that the Fibonacci I blade profile is the most suitable since it presents the highest SC_{Pmax}.

Table 3. SCpmax corresponding to Savonius, Fibonacci I, and Fibonacci II.

Blade Profile	C_{Pmax}	C_F at P Max	SC_{Pmax}
Savonius	0.217	0.2614	0.415
Fibonacci I	0.243	0.2886	0.421
Fibonacci II	0.205	0.2494	0.411

3.2. Design Aspects in the Fibonacci Blade Profile

Once the superiority of the Fibonacci blade profile over the Savonius one was demonstrated, this section aims to optimize the Fibonacci blade profile. To this end, the effect of several parameters is analyzed. These parameters are the number of blades, aspect ratio, overlap, separation gap, and twist angle.

3.2.1. Effect of the Number of Blades

The effect of the number of blades is shown in Figure 12. It can be seen that the power coefficients obtained with three blades are lower than those obtained with two blades. Using four blades, the power coefficients are even lower. The reason is that a blade deflects the air flow that would focus on the next blade that, in turn, also deflects the air flow that could focus on the next blade after it. Each blade affects the following one, and the result is that less energy from the moving air is converted into mechanical energy.

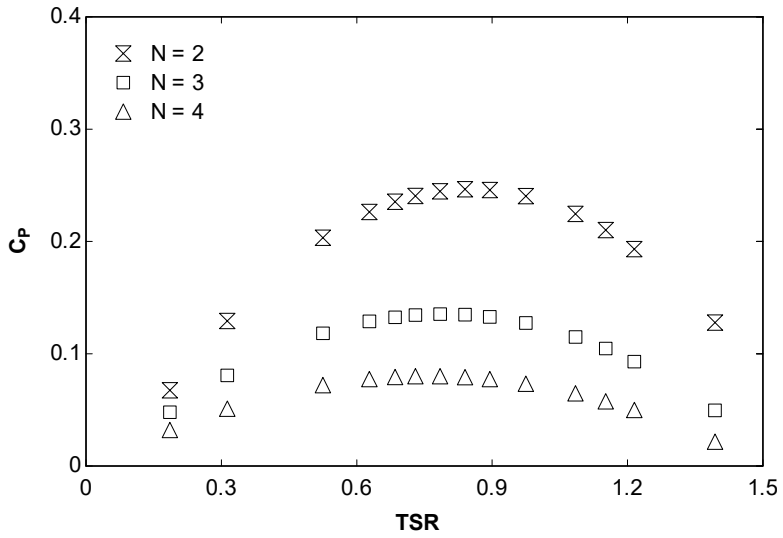

Figure 12. C_P against TSR for 2, 3, and 4 blades. AR = 1, O = 0, SG = 0, TA = 0.

As mentioned above, an advantage of turbines with more than two blades is that the starting torque is lower. This is especially important under low velocity wind conditions, where turbines with more than two blades are appropriate although they provide less efficiency.

3.2.2. Effect of the Aspect Ratio

The effect of the aspect ratio is shown in Figure 13. It can be seen that the power coefficients increase with the aspect ratio until AR = 7. Nevertheless, above this value of the aspect ratio the power coefficients decrease again. On the one hand, the power coefficients increase with the aspect ratio due to a reduction of end blade losses. On the other hand, the endplates increase the efficiency of the turbine due to the reduced escaping of air, but this effect is reduced when the aspect ratio is increased. These opposed effects lead to an optimum value of the aspect ratio. In particular, Figure 13 shows an increment of 31.2% of the average power coefficient using AR = 7.

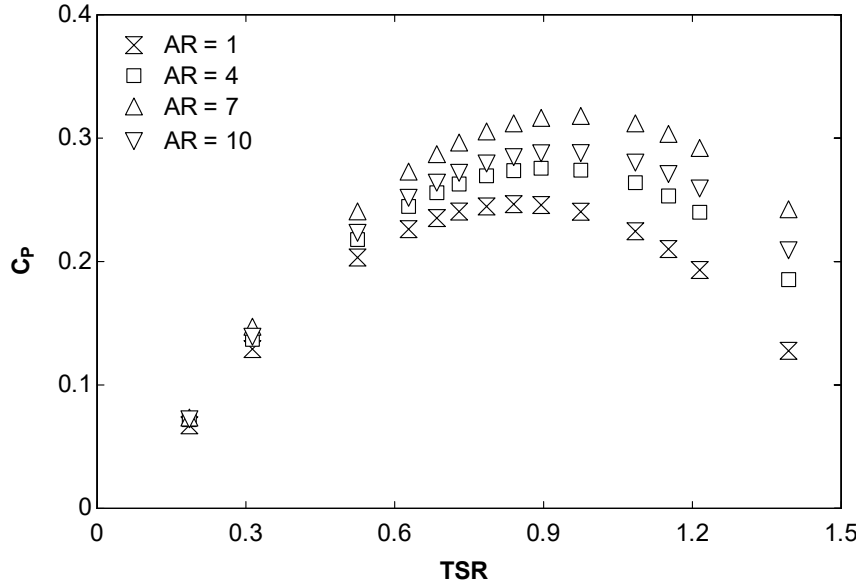

Figure 13. C_P against TSR for aspect ratios 1, 4, 7, and 10. N = 2, O = 0, SG = 0, TA = 0.

3.2.3. Effect of the Overlap

The effect of the overlap is shown in Figure 14. It is habitual to represent this parameter as O/C, i.e., the relation between the overlap and chord length. It can be seen that the most appropriate overlap value is 0.15. The overlap provides a spacing between the blades, which allows the passage of air from the advancing to the returning blade. This air may lead to increments of the power depending on the overlap value.

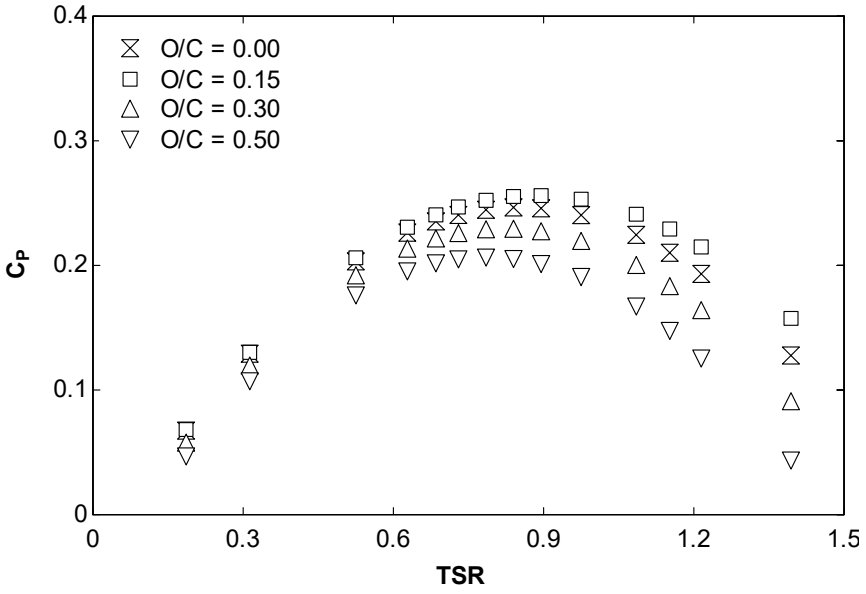

Figure 14. C_P against TSR for overlap–chord length relation 0, 0.15, 0.3, and 0.5. N = 2, AR = 1, SG = 0, TA = 0.

The phenomena caused by the overlap parameter is shown in Figure 15. It can be seen that the overlap may increment the power coefficients because the air flows from the advancing blade for the returning blade, increasing the pressure on the convex side. This helps the convex side to produce power. Nevertheless, high overlaps lead to an excessive reduction of air on the concave side of the blades, which reduces the power coefficients.

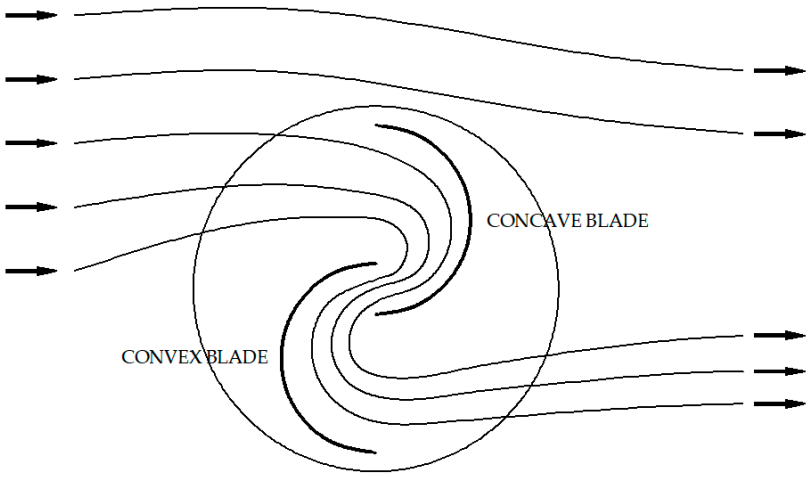

Figure 15. Working principle of the Fibonacci turbine with overlap.

3.2.4. Effect of the Separation Gap

The effect of the separation gap is shown in Figure 16. As in the previous case, it is habitual to represent this parameter as SG/C, i.e., the relation between the separation gap and chord length. It can be seen that a zero separation gap provides the highest power coefficients. The reason is that the separation inappropriately directs the air on the convex side of the returning bucket, reducing the power coefficient.

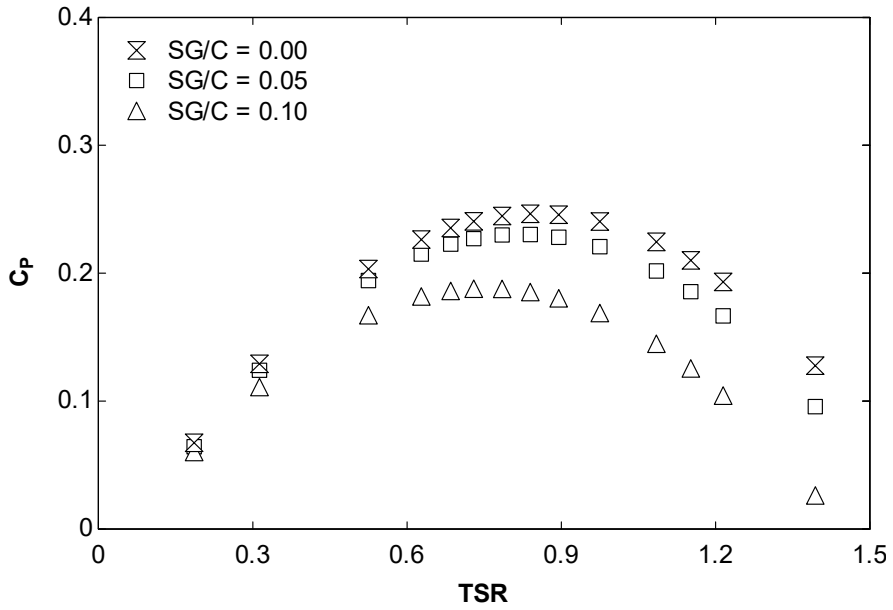

Figure 16. C_P against TSR for separation gap–chord length relation 0, 0.05, and 0.1. N = 2, AR = 1, O = 0, TA = 0.

The phenomena caused by the separation gap parameter is shown in Figure 17. It can be seen that the separation gap could increment the power if the pressure created on the convex side would acquire a value large enough to promote torque and thus power on this convex side. Nevertheless, the flow path is not able to promote torque and thus power on this side. The flow that passes from the concave to the convex blade is wasted and thus the power is reduced as the separation gap is increased.

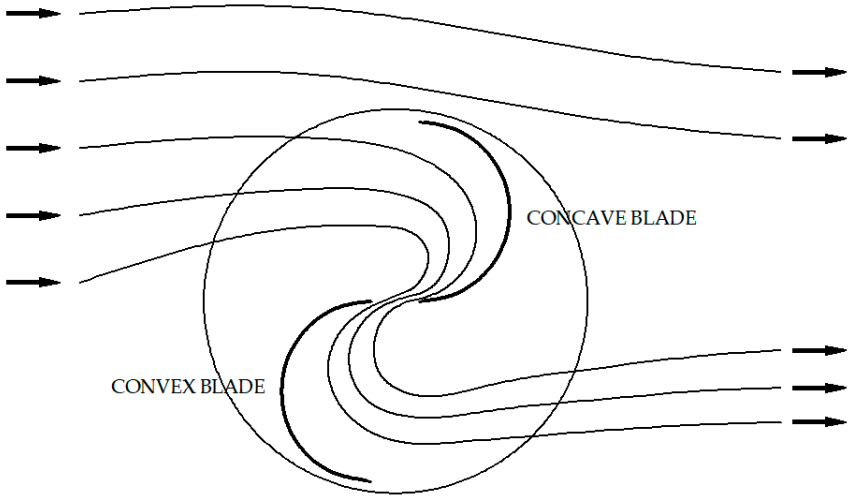

Figure 17. Working principle of the Fibonacci turbine with separation gap.

3.2.5. Effect of the Twist Angle

The effect of the twist angle is shown in Figure 18. It can be seen that a certain value of twist angle is positive since the power coefficients are increased. With 90° value the power coefficients are higher than those corresponding to 0°. If the twist angle is increased to 180° the power coefficients are higher. The geometry corresponding to 180° is shown in the figure. On the other hand, excessive twist angles, in this case 270°, reduce the power coefficient.

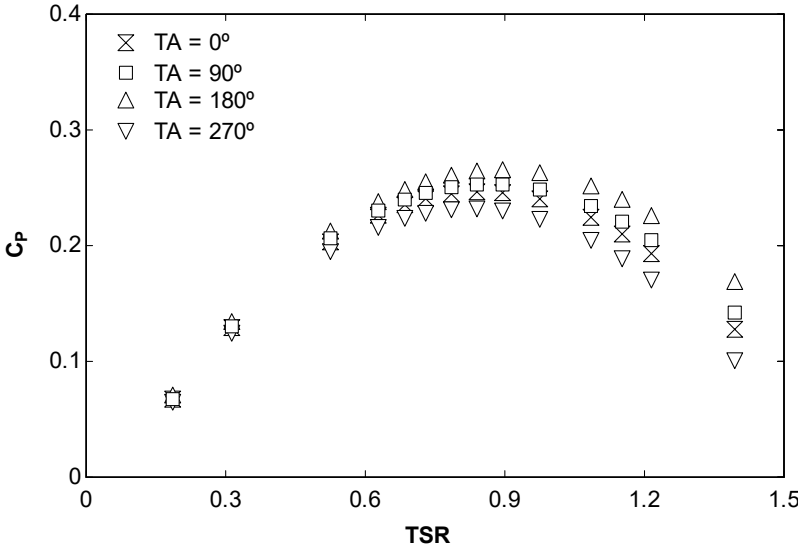

Figure 18. C_P against TSR for twist angles 0°, 90°, 180°, and 270°. N = 2, AR = 1, O = 0, SG = 0.

4. Conclusions

The present work proposes an improvement of the Savonius turbine. The Savonius turbine is based on semi-circular blade profiles, while the present work proposes a nature-inspired shape based on the Fibonacci spiral. This shape is presented repeatedly in nature. A numerical model based on CFD was created to compare the Fibonacci and Savonius blade profiles and obtained better results for the Fibonacci shape. An improvement of 14.1% on the average power coefficient and 13.5% on the average thrust coefficient were obtained with the Fibonacci blade profile. After that, the effect of the number of blades, separation gap, aspect ratio, overlap, and twist angle was investigated. The main findings of the present work are:

- The optimum number of blades are two;
- The optimum aspect ratio is seven.
- The optimum overlap/chord length relation is 0.15.
- The optimum separation gap is 0.
- The optimum twist angle is 180°.

The findings regarding the optimum number of blades and separation gap are in line to the scientific literature about regular Savonius turbines. Nevertheless, regarding optimum aspect ratio, overlap, and twist angle, there is no consensus in the literature.

For future works, an important aspect is to design a turbine with the most appropriate combination of number of blades, aspect ratio, overlap, separation gap, and twist angle. To this end, optimization models will be employed in future works, such as Multidisciplinary Design Optimization (MDO) algorithms or Artificial Neural Networks (ANN). Another future research will lay on further improve the performance of the Savonius turbine based on the Fibonacci blade profile by means of improvements, such as V-shape deflectors, deflecting plates, curtains, venting slots, guide vanes, several stages, and combinations of Savonius–Darrieus turbines. Once the most appropriate VAWT design is obtained, another necessary area of research will be the economic aspect. Feasibility analysis will be realized in future works to compute the economic advantages of using VAWT in urban environments.

Author Contributions: Conceptualization, J.B.D., J.d.D.R.G., A.C.C., J.T.M., C.G.C. and M.I.L.G.; methodology, J.B.D., J.d.D.R.G., A.C.C., J.T.M., C.G.C. and M.I.L.G.; software, J.B., J.d.D.R.G., A.C.C., J.T.M., C.G.C. and M.I.L.G.; validation, J.B., J.d.D.R.G., A.C.C., J.T.M., C.G.C. and M.I.L.G.; formal analysis, J.B., J.d.D.R.G., A.C.C., J.T.M., C.G.C. and M.I.L.G.; investigation, J.B., J.d.D.R.G., A.C.C., J.T.M., C.G.C. and M.I.L.G.; resources, J.B.D., J.d.D.R.G., A.C.C., J.T.M., C.G.C. and M.I.L.G.; writing—original draft preparation, M.I.L.G.; writing—review and editing, J.B.D., J.d.D.R.G., A.C.C., J.T.M. and C.G.C.; supervision, J.B.D., J.d.D.R.G., A.C.C., J.T.M., C.G.C. and M.I.L.G. All authors have read and agreed to the published version of the manuscript.

Funding: This research received no external funding.

Institutional Review Board Statement: Not applicable.

Informed Consent Statement: Not applicable.

Conflicts of Interest: The authors declare no conflict of interest.

References

1. Liu, Y.; Xiao, Q.; Atilla, I.; Peyard, C.; Wan, D. Establishing a fully coupled CFD analysis tool for floating offshore wind turbines. *Renew. Energy* **2017**, *112*, 280–301. [CrossRef]
2. Liu, Z.; Tu, Y.; Wang, W.; Qian, G. Numerical analysis of a catenary mooring system attached by clump masses for improving the wave-resistance ability of a spar buoy-type floating offshore wind turbine. *Appl. Sci.* **2019**, *9*, 1075. [CrossRef]
3. Blanco, J.; Lamas, M.I.; Couce, A.; Rodriguez, J.D. Vertical Axis Wind Turbines: Current Technologies and Future Trends. In Proceedings of the International Conference on Renewable Energies and Power Quality, A Coruña, Spain, 25–27 March 2015.
4. Pagnini, L.C.; Burlando, M.; Repetto, M.P. Experimental power curve of small-size wind turbines in turbulent urban environment. *Appl. Energy* **2015**, *154*, 112–121. [CrossRef]
5. Vita, G.; Šarkić-Glumac, A.; Hemida, H.; Salvadori, S.; Baniotopoulos, C. On the wind energy resource above high-rise buildings. *Energies* **2020**, *13*, 3641. [CrossRef]
6. Wijayanto, R.P.; Kono, T.; Kiwata, T. Performance characteristics of an orthopter-type vertical axis wind turbine in shear flows. *Appl. Sci.* **2020**, *10*, 1778. [CrossRef]
7. Savonius, S.J. The S-rotor and its applications. *Mech. Eng.* **1931**, *53*, 333–338.
8. Talukdar, P.K.; Sardar, A.; Kulkarni, V.; Saha, U.K. Parametric analysis of model Savonius hydrokinetic turbines through experimental and computational investigations. *Energy Convers. Manag.* **2018**, *158*, 36–49. [CrossRef]
9. Zhang, Y.; Kang, C.; Zhao, H.; Teng, S. Effects of in-line configuration of drag-type hydrokinetic rotors on inter-rotor flow pattern and rotor performance. *Energy Convers. Manag.* **2019**, *196*, 44–55. [CrossRef]
10. Alipour, R.; Alipour, R.; Koloor, S.S.R.; Petru, M.; Ghazanfari, S.A. On the Performance of Small-Scale Horizontal Axis Tidal Current Turbines. Part 1: One Single Turbine. *Sustainability* **2020**, *12*, 5985. [CrossRef]
11. Alipour, R.; Alipour, R.; Fardian, F.; Koloor, S.S.R.; Petru, M. Performance improvement of a new proposed Savonius hydrokinetic turbine: A numerical investigation. *Energy Rep.* **2020**, *6*, 3051–3066. [CrossRef]

12. Akwa, J.V.; Vielmo, H.A.; Petry, A.P. A review on the performance of Savonius wind turbines. *Renew. Sustain. Energy Rev.* **2012**, *16*, 3054–3064. [CrossRef]
13. Tian, W.; Song, B.; VanZwieten, J.; Pyakurel, P. Computational fluid dynamics prediction of a modified Savonius wind turbine with novel blade shapes. *Energies* **2015**, *8*, 7915–7929. [CrossRef]
14. Pujol, T.; Massaguer, A.; Massaguer, E.; Montoro, L.; Comamala, M. Net power coefficient of vertical and horizontal wind turbines with crossflow runners. *Energies* **2018**, *11*, 110. [CrossRef]
15. Vance, W. Vertical Axis Wind Rotors—Status and potential. In Proceedings of the Conference on Wind Energy Conversion Systems, Washington, DC, USA, 11–13 June 1973; pp. 96–102.
16. Saha, U.K.; Thotla, S.; Maity, D. Optimum design configuration of Savonius rotor through wind tunnel experiments. *J. Wind Eng. Ind. Aerodyn.* **2008**, *96*, 1359–1375. [CrossRef]
17. Alexander, A.J.; Holownia, B.P. Wind tunnel tests on a savonius rotor. *J. Wind Eng. Ind. Aerodyn.* **1978**, *3*, 343–351. [CrossRef]
18. Zhao, Z.; Zheng, Y.; Xu, X.; Liu, W.; Hu, G. Research on the Improvement of the Performance of Savonius Rotor Based on Numerical Study. In Proceedings of the 2009 International Conference on Sustainable Power Generation and Supply, Nanjing, China, 6–7 April 2009; pp. 1–6. [CrossRef]
19. Sheldahl, R.E.; Blackwell, B.F.; Feltz, L.V. Wind tunnel performance data for two- and three-bucket Savonius rotors. *J. Energy* **1978**, *2*, 160–164. [CrossRef]
20. Fujisawa, N. On the torque mechanism of Savonius rotors. *J. Wind Eng. Ind. Aerodyn.* **1992**, *40*, 277–292. [CrossRef]
21. Mojola, O.O. On the aerodynamic design of the savonius windmill rotor. *J. Wind Eng. Ind. Aerodyn.* **1985**, *21*, 223–231. [CrossRef]
22. Menet, J.L.; Bourabaa, N. Increase in the Savonius rotors efficiency via a parametric investigation. In Proceedings of the European Wind Energy Conference, London, UK, 22–25 November 2004.
23. Lee, J.H.; Lee, Y.T.; Lim, H.C. Effect of twist angle on the performance of Savonius wind turbine. *Renew. Energy* **2016**, *89*, 231–244. [CrossRef]
24. Damak, A.; Driss, Z.; Abid, M.S. Experimental investigation of helical Savonius rotor with a twist of 180°. *Renew. Energy* **2013**, *52*, 136–142. [CrossRef]
25. Damak, A.; Driss, Z.; Abid, M.S. Optimization of the helical Savonius rotor through wind tunnel experiments. *J. Wind Eng. Ind. Aerodyn.* **2018**, *174*, 80–93. [CrossRef]
26. Kumar, G.; Ram, V.R.; Kumar, N. Numerical analysis of different blade profile of wind turbine. *Int. J. Appl. Eng. Res.* **2018**, *6*, 375–385.
27. Alom, N.; Saha, U.K. Influence of blade profiles on Savonius rotor performance: Numerical simulation and experimental validation. *Energy Convers. Manag.* **2019**, *186*, 267–277. [CrossRef]
28. Kacprzak, K.; Liskiewicz, G.; Sobczak, K. Numerical investigation of conventional and modified Savonius wind turbines. *Renew. Energy* **2013**, *60*, 578–585. [CrossRef]
29. Benesh, A.H. Wind Turbine System Using a Savonius-Type Rotor. U.S. Patent 5494407A, 27 February 1996.
30. Mohamed, M.H.; Janiga, G.; Pap, E.; Thévenin, D. Optimal blade shape of a modified Savonius turbine using an obstacle shielding the returning blade. *Energy Convers. Manag.* **2011**, *52*, 236–242. [CrossRef]
31. Chan, C.M.; Bai, H.L.; He, D.Q. Blade shape optimization of the Savonius wind turbine using a genetic algorithm. *Appl. Energy* **2018**, *213*, 148–157. [CrossRef]
32. Lamas Galdo, M.I.; Rodriguez Vidal, C.G. Hydrodynamics of biomimetic marine propulsion and trends in computational simulations. *J. Mar. Sci. Eng.* **2020**, *8*, 479. [CrossRef]
33. Lamas, M.I.; Rodríguez, C.G.; Rodríguez, J.D. Optimization of the efficiency of a biomimetic marine propulsor using CFD. *Ing. E Investig.* **2014**, *34*, 17–21.
34. Lamas, M.I.; Rodríguez, J.D.; Rodríguez, C.G. CFD analysis of biologically-inspired marine Propulsors. *Brodogradnja* **2012**, *63*, 125–133.
35. Lamas, M.I.; Rodríguez, J.D.; Rodríguez, C.G.; González, P.B. Three-dimensional CFD analysis to study the thrust and efficiency of a biologically-inspired marine propulsor. *Pol. Marit. Res.* **2011**, *18*, 10–16. [CrossRef]
36. U.S. National Oceanic and Atmospheric Administration. *Public Domain.* Available online: https://commons.wikimedia.org/wiki/File:Fran10.jpg (accessed on 10 July 2022).
37. NASA; ESA. The Hubble Heritage Team (STScI/AURA). In *Public Domain*. Available online: https://commons.wikimedia.org/wiki/File:The_Two-faced_Whirlpool_Galaxy.jpg (accessed on 10 July 2022).
38. Blanco, J.; Rodriguez, J.D.; Couce, A.; Lamas, M.I. Proposal of a nature-inspired shape for a vertical axis wind turbine and comparison of its performance with a semicircular blade profile. *Appl. Sci.* **2021**, *11*, 6198. [CrossRef]
39. Altan, B.D.; Atılgan, M. An experimental and numerical study on the improvement of the performance of Savonius wind rotor. *Energy Convers. Manag.* **2008**, *49*, 3425–3432. [CrossRef]
40. Plourde, B.D.; Abraham, J.P.; Mowry, G.S.; Minkowycz, W.J. Simulations of three-dimensional vertical-axis turbines for communications applications. *Wind Eng.* **2012**, *36*, 443–453. [CrossRef]
41. Gallo, L.A.; Chica, E.L.; Flórez, E.G.; Obando, F.A. Numerical and experimental study of the blade profile of a Savonius type rotor implementing a multi-blade geometry. *Appl. Sci.* **2021**, *11*, 10580. [CrossRef]
42. Zhang, H.; Li, Z.; Xin, D.; Zhan, J. Improvement of aerodynamic performance of Savonius wind rotor using straight-arc curtain. *Appl. Sci.* **2020**, *10*, 7216. [CrossRef]

43. Akwa, J.V.; Alves da Silva Júnior, G.; Petry, A.P. Discussion on the verification of the overlap ratio influence on performance coefficients of a Savonius wind rotor using computational fluid dynamics. *Renew. Energy* **2012**, *38*, 141–149. [CrossRef]
44. Blanco Damota, J. Perfil de Pala de Turbina Eólica de Eje Vertical de Diseño Bioinspirado: Estudio Comparativo y Optimización Mediante Modelo CFD Parametrizado. Ph.D. Thesis, Unviersidade da Coruña, A Coruña, Spain, 2022.
45. Ross, I.; Altman, A. Wind tunnel blockage corrections: Review and application to Savonius vertical-axis wind turbines. *J. Wind Eng. Ind. Aerodyn.* **2011**, *99*, 523–538. [CrossRef]
46. Parmanand, S. The So-called Fibonacci numbers in ancient and medieval India. *Hist. Math.* **1985**, *12*, 229–244. [CrossRef]
47. Huntley, H.E. *The Divine Proportion*; Dover Publications Inc.: New York, NY, USA, 1970.
48. Kamoji, M.A.; Kedare, S.B.; Prabhu, S.V. Experimental investigations on single stage modified Savonius rotor. *Appl. Energy* **2009**, *86*, 1064–1073. [CrossRef]
49. Tartuferi, M.; D'Alessandro, V.; Montelpare, S.; Ricci, R. Enhancement of Savonius wind rotor aerodynamic performance: A computational study of new blade shapes and curtain systems. *Energy* **2015**, *79*, 371–384. [CrossRef]
50. Ostos, I.; Ruiz, I.; Gajic, M.; Gómez, W.; Bonilla, A.; Collazos, C. A modified novel blade configuration proposal for a more efficient VAWT using CFD tools. *Energy Conv. Manag.* **2019**, *180*, 733–746. [CrossRef]
51. Sharma, S.; Sharma, R.K. Performance improvement of Savonius rotor using multiple quarter blades—A CFD investigation. *Energy Convers. Manag.* **2016**, *127*, 43–54. [CrossRef]
52. Chehouri, A.; Younes, R.; Ilinca, A.; Perron, J. Review of performance optimization techniques applied to wind turbines. *Appl. Energy* **2015**, *142*, 361–388. [CrossRef]
53. Alipour, R.; Alipour, R.; Fardian, F.; Tahan, M.H. Optimum performance of a horizontal axis tidal current turbine: A numerical parametric study and experimental validation. *Energy Conv. Manag.* **2022**, *258*, 115533. [CrossRef]